Journal of Catalysis **185,** 223–235 (1999)
Article ID jcat.1999.2520, available online at http://www.idealibrary.com on IDEAL®

Dark- and Photoreactions of Ethanol and Acetaldehyde over TiO_2/Carbon Molecular Sieve Fibers

T. Reztsova,* C.-H. Chang,* J. Koresh,† and H. Idriss*,[1]

*Materials Chemistry, Department of Chemistry, The University of Auckland, Auckland, New Zealand;
†Nuclear Research Center, Negev, P.O. Box 9001, Beer Sheva, Israel

Received February 16, 1999; revised April 7, 1999; accepted April 13, 1999

TiO_2 has been synthesized within the pores of carbon molecular sieve fibers (CMSF) in order to grow particles of quantum size. TiO_2/CMSF characteristics were followed by X-ray photoelectron spectroscopy (XPS), X-ray diffraction (XRD), and UV–vis diffuse reflectance. XPS showed that all Ti cations are in a $+4$ oxidation state. The reduction profile of Ti cations (made by preferential O anion removal due to Ar^+ sputtering), as evidenced by Ti^{+x}/Ti^{+4} cations, is very similar to that already observed for well-defined TiO_2 surfaces. The absence of XRD pattern indicated that TiO_2 particles are in an amorphous form. UV–vis diffuse reflectance showed a considerable blue shift ($\Delta E = 0.6$–0.7 eV) of the band gap of TiO_2/CMSF when compared to TiO_2 (anatase). This shift translates an average particle radius of 15 ± 2 Å. Larger TiO_2 particles, outside the CMSF nanopores, are, however, observed by TEM. Dark- and photoreactions of ethanol and acetaldehyde have been investigated over TiO_2/CMSF by steady state kinetics and temperature programmed desorption in UHV conditions, as well as in batch conditions at atmospheric pressure. UHV-steady state ethanol reactions have shown eightfold increase in the reaction rate at 573 K in the presence of UV when compared to dark reactions at the same temperatures. The rate constants ratio k_2K_2/k_1K_1, for the photoreactions of ethanol, is ca. 40 times higher for TiO_2/CMSF than for TiO_2 (powder) indicating the high selectivity of the former toward total conversion of ethanol to CO_2 with minor accumulation of acetaldehyde (k_1K_1 and k_2K_2 are the rate constants for ethanol to acetaldehyde and acetaldehyde to CO_2, respectively). Evidence of C–C bond dissociation is given by formaldehyde desorption during UV-acetaldehyde-TPD over TiO_2/CMSF under UHV conditions. Moreover, UV-acetaldehyde-TPD indicated a twofold increase of the reductive coupling product (butadiene). The latter requiring Ti^{+x} ($x < 4$) to be formed translates an increase of Ti^{+x} populations under UV illumination.

INTRODUCTION

Photocatalytic degradation of organic compounds using semiconductors has been the subject of extensive studies the past two decades (1–10). The most active and efficient semiconductor known to date is TiO_2. Although the exact reasons for this are not yet fully understood, both the catalytic activity and in particular the stability of this oxide semiconductor is unique when compared to other wide band-gap oxide semiconductors. The majority of photocatalytic reactions have been conducted on suspended TiO_2 particles in aqueous or organic environments (9) for direct environmental applications. Relatively less work, however, has been conducted on solid–gas photocatalytic reactions, although due to potential indoor decontamination processes this field of investigation is quickly growing. Solid–gas photocatalytic reactions are usually devoted to kinetics, surfaces, and surface–adsorbates spectroscopic studies. The common forms of TiO_2 are anatase, rutile, and brookite; the last is relatively less studied (11). The photocatalytic reactions of organic compounds over anatase and rutile surfaces have been studied. In particular oxygenated and chlorinated compounds have been investigated on the surfaces of TiO_2 under dark and UV conditions. Among oxygenates the reactions of alcohols were studied on TiO_2 powder and single crystal by several techniques, such as temperature programmed desorption (TPD)–dark reactions (12–14), steady state kinetics–dark reactions (15) and photoreactions (16–18), infrared spectroscopy–dark reactions (19) and photoreactions (20), X-ray photoelectron spectroscopy (12)–dark reactions, and Raman spectroscopy–dark reactions (21, 22). Ethanol reactions on oxide surfaces including TiO_2 have received considerable attention. The reasons for this are multiple. These include: (i) syngas conversion to ethanol on metal-doped oxide materials, such as Rh deposited on TiO_2 (23); (ii) oxidative dehydrogenation of ethanol to acetaldehyde (15), the latter is converted to crotonaldehyde (an unsaturated aldehyde) via β-aldolization reaction (24); (iii) the use of ethanol as a fuel additive (25, 26); (iv) as a method of monitoring the dehydration (to ethylene) versus dehydrogenation (to acetaldehyde) activity of a given catalytic material (27, 28); (v) photodecomposition of ethanol over TiO_2 surfaces, as an example of organic tropospheric pollutants (16–18); and (vi) more recently, ethanol has also been seriously considered as a viable pure source for green

[1] To whom correspondence should be addressed.

0021-9517/99 $30.00

H_2-production, particularly because ethanol can be manufactured from biomass (29–31).

Under dark conditions, ethanol dissociates on TiO_2 powder to ethoxy species at room temperature and above (12–14). Ethoxy species undergo dehydrogenation to acetaldehyde, the main reaction product, as well as dehydration to ethylene (12–15). No direct evidence of ethanol oxidation to acetate species has been reported; although, small amounts of acetone, presumably through acetate ketonization, were observed as a secondary reaction on TiO_2 (15). This is unlike ZnO, another wide band-gap semiconductor, whose band-gap energy has the same value as TiO_2 (3.2 eV) (32, 33), but where adsorption of methanol or ethanol resulted in the formation of formate (34) or acetate (35) species, respectively. It is worth mentioning that small amounts of acetates have recently been reported by IR on TiO_2 powder from acetaldehyde (36).

Photoreactions of ethanol on TiO_2 have been studied by several workers (16–18). Clearly TiO_2 yields CO_2 as a final product. The initial reaction mechanism involves the following steps. (a) When TiO_2 is excited with energy equal to (or higher than) its band gap (ca. 3.2 eV) electron transfer from the valence band (O 2*p*) to the conduction band (Ti 3*d*) occurs. (b) As a result electron/hole pairs are formed in the conduction/valence band region. (c) In the presence of oxygen and/or H_2O superoxide ($^{\cdot}O_2$) and/or hydroxyl ($^{\cdot}OH$) radicals are formed. (d) These radicals attack adsorbed organic species (ethoxides) on the surface of TiO_2 and decompose them. (e) Several reaction intermediates have been observed, such as acetaldehyde (37), formaldehyde (38), methanol (37), and formic and acetic acids (18).

The reaction is, however, sensitive to bulk structure. Anatase TiO_2 is far more active than the rutile (37, 39). This is unlike the dark reaction where no dramatic effects were observed (40). Surface defects are another property that may well play an important role in the enhancement of reaction rates (41). Although this has been reported on rutile TiO_2 (110) single crystal containing defects (42), it has not been conclusively observed on TiO_2 powders (37).

Another important aspect of semiconductors is their quantum size effects (43–46). When the crystallite dimensions of a semiconductor fall below a critical radius of approximately 10 nm, the charge carriers behave as a sample particle in a box. Two characteristics result from this confinement: (1) The band gap increases and (2) the band edge shifts to yield larger redox potentials (47). As a result the rate constant of charge transfer increases (48–50). This infers that the use of size quantized semiconductor particles may result in increased photoefficiencies for systems in which the rate limiting step is charge transfer. Another important implication of decreasing the size of semiconductor particles is increasing the surface to bulk ratio. Upon excitation electron/hole pairs are formed and bulk electrons and holes migrating to the semiconductor surface will participate in the reaction (in addition to surface electron/hole pairs). This process is in competition with electron/hole recombination. Bulk electron/hole recombination will thus decrease with increasing the surface to bulk ratio and this may result in enhancement of the reaction rate. In fact, femtosecond diffuse reflection spectroscopy experiments of *Q*-sized and P-25 (Degussa) TiO_2 powders have shown that the *Q*-sized TiO_2 displayed the largest fraction of long-lived electrons (51).

There are several methods for preparing nanoclusters of semiconductors. For example, direct synthesis of CdS within the pore structure of zeolites leads to discrete $(CdS, O)_4$ cubes located within the small sodalite units (52). Other nanoclusters have been synthesized by the method of controlled cluster fusion (53, 54). Another method of preparing TiO_2 nanoparticles is based on the sol–gel (2D) process (55). As a result a nanometer thick TiO_2 film composed of quantum-sized particles has been prepared. Carbon molecular sieve fibers (CMSF) are potential hosts for TiO_2 because of their stability (56–60), uniformity, and more important because they are chemically inert (thus stable). Unlike zeolite materials (usually having acid properties) ultramicroporous carbon surfaces do not contain Brønsted acid sites; these would alter the chemical properties of the oxide semiconductor. In other words the oxygen anions of small TiO_2 particulates within the pore structure of the CMSF may not be dramatically affected. CMSF are amorphous materials that contain graphite regions. The ability to discriminate between adsorbing molecules on the basis of size and shape is achieved by the existence of constrictions originated from the graphite interlayer distance. Molecules smaller than the constriction size can rapidly diffuse through them into the associated micropore volume, while molecules with larger dimensions cannot penetrate (61, 62). A small change in the effective size of the constrictions can largely affect the diffusion rate (62, 63). The constrictions are, on one hand, low-energy adsorption sites, because of steric interactions of pore walls with the adsorbate molecules. On the other hand, these sites are kinetically protracted (56). Previous studies (64) have shown significant effect of constrictions tailoring on the selectivity of Pt on CMSF catalyst. Usually high shape selectivity decreases the catalytic activity because of slower diffusion of the reactant or product inside the porous structure. On the other hand, the active sites of these catalysts are protected from cocking processes or conglomeration of the active material and, therefore, the catalysts exhibit much higher stability.

This work presents a study of the reaction of ethanol and acetaldehyde over TiO_2 powder (anatase) and TiO_2/CMSF. The TiO_2/CMSF has been characterized by XPS, XRD, UV-vis diffuse reflectance, and TEM. The reaction kinetics has been followed by temperature programmed desorption and under steady state conditions.

EXPERIMENTAL

A. Preparation of TiO_2/CMSF

The CMSF are TCM 128, used as received, produced by Carbone-Lorraine, France. The CMSF was evacuated to 10^{-2} Torr, to remove the adsorbed water, for several hours. Titanium ethoxide was then introduced to dope the CMSF sample. After 15 min the sample was transferred to a glass tube where wetted nitrogen was flushed through for 1 h to transform titanium ethoxide to titanium hydroxide. The titanium hydroxide was then decomposed to titanium oxide by heating the sample to 473 K for 2 h in a dry nitrogen flow.

B. Temperature Programmed Desorption (TPD)

TPD experiments were conducted in a stainless steel ultrahigh vacuum (UHV) chamber equipped with a Varian ion pump (220 L/s), a Balzer turbo pump (240 L/s), a Φ ion sputter gun, a Spectra Vision Quadrupole mass spectrometer (scanning up to 200 amu) with a scanning rate of 12 masses/10 s, and a heating stage for sample treatment (up to ca. 850 K). The sample was mounted horizontally on a Ta foil (0.125 mm thick) heated with Ta wires (0.5 mm thick). A type K thermocouple spot-welded to the Ta foil was used to measure the sample temperature. The pressure of the chamber was in the low 10^{-9} Torr under operating conditions. Ethanol was contained in a glass to metal tube connected to a dosing line with a base pressure of ca. 10^{-2} Torr. Ethanol was cleaned by freeze–pump–thaw cycles and its purity was checked by the quadrupole mass spectrometer. The sample (1 cm^2, 20 mg having a total surface area of ca. 8 m^2) was cleaned by successive heating (800 K) and Ar^+-sputtering cycles (3 kV; 25 mA) until blank TPD showed no desorption of m/e 28 (CO) and 44 (CO_2) up to 750 K. The sample surface was then assumed to be clean. Dosing of ethanol was performed at ca. 10^{-7} Torr for 5 min (30 L). Photoexcitation was performed via a defocused 100 W Hg-lamp (the same one was used for catalytic reactions) with an incident angle of 45° to the sample (at 20 cm from the UV lamp). The flux of ultraviolet photons was calibrated by a standard actinometric method and was found to be ca. $2 \pm 1 \times 10^{15}$ photons/cm^2 s (ca. four times less than a typical noontime midlatitude solar flux). After pumping down for ca. 1 h, TPD was started with a ramping rate of 0.8 K/s. The following masses were monitored in separate runs (2, 12, 15–18, 24–32, 36–46, 55–72, 77, 78 and 88). The TPD yield was calculated as described before (65); mass spectrometer correction factors were computed as indicated elsewhere (66).

C.i. Photocatalytic Reactions at Atmospheric Pressure

Reactions proceeded in a small Pyrex batch reactor excited with the same 100 W Hg-lamp described above. Forced-air cooling kept the reactor temperature at ≈300 K. Reactions continued in air at 50% relative humidity. Previous work has shown that water partial pressure affected the reaction rate constant (although not dramatically) of ethanol decomposition on TiO_2 anatase [the rate constant increased by about 50% at 30% humidity (17), when compared to that at 0% humidity]. Reactant concentrations ranged from 10^{-9} to 10^{-8} mol/mL. A gas chromatograph with flame ionization detection (FID) monitored the reaction products. Products were separated using a Chromosorb 102 packed column (o.d. = 1/8″, l = 6 feet).

C.ii. Photocatalytic Reactions in Ultrahigh Vacuum (UHV)

The same apparatus described in section B is used for the steady state reaction in UHV. A dosing pressure of ethanol of ca. 5×10^{-7} Torr was used. Reactant and products were monitored by the quadrupole mass spectrometer. The sample was subject to subsequent treatments similar to those in section B.

D. X-Ray Photoelectron Spectroscopy (XPS)

XPS was performed using a Kratos XSAM-800 model with a base pressure of ca. 10^{-9} Torr. Ti(2*p*), O(1*s*), and C(1*s*) regions were scanned each run. The TiO_2/CMSF sample (ca. 1 cm^2) was loaded without further treatments. Ar ion sputtering was performed using a direct beam Kratos ion gun at a pressure of ca. 5×10^{-7} Torr (emission current = 25 mA and accelerating voltage = 3 kV). Mg$K\alpha$ radiation was used at 170 W. Collection of the spectra were conducted at a pass energy of 38 eV. No sample charging was observed.

E. TEM

Specimens were prepared by embedding TiO_2/CMSF in EM-Bed 812 Epoxy resin that was allowed to polymerize into a block at 330 K for 48 h. To determine the mean dimension of the TiO_2 particles, specimens with Epoxy resin of approximate 500 nm thickness were first trimmed by hand with a sharp razor and then cut with a Diatom diamond knife on LKB Ultracut Ultramicrotome which allows ultrathin sections of 80 nm to be obtained. TEM experiments were performed using a Philips CM 12 that provides accelerating voltage in the range 20–120 kV and magnifications from 30,000 to 600,000×. Exposure time varied between 1.5 and 3 s.

F. UV–Vis Diffuse Reflectance

UV–vis spectra were performed using a Shimadzu double-beam spectrophotometer UV-2100. The UV spectrophotometer was equipped with an integrating sphere, having a 60 mm internal diameter, and a photomultiplier R-446U detector. Spectra were measured in the range 240–500 nm at a slit width of 2 nm. The incident angle of the reflecting beam to the sample was 8°. Initially, TiO_2/CMSF

sample (0.035 g) was finely ground which was then mixed with $BaSO_4$ followed by pressing into a sample retainer. However, this procedure gave rise to a very weak ionic oxide absorption. Therefore a different method of preparing the UV sample was employed: TiO_2/CMSF sample was imprinted onto anhydrous barium sulfate powder, which was used as a support for UV reflectance spectroscopy. The baseline was done using $BaSO_4$ as the reference.

RESULTS

1. XPS of TiO_2/CMSF

Figure 1a presents the XPS Ti(2*p*) region of TiO_2/CMSF. Ti($2p_{3/2}$) and Ti($2p_{1/2}$) lines at 459.3 (FWHM 1.2 eV) and 465.0 eV (FWHM 2.2 eV) were observed, respectively. The lines positions and the FWHM clearly indicate that all the Ti cations are in +4 oxidation state. This is in agreement with several previous reports on TiO_2 powder and single crystals (67–71). Detailed studies of the effect of sputtering on TiO_2 surfaces have been reported elsewhere (67–70); briefly a fraction of Ti^{+4} cations is reduced to Ti^{+x} ($0 < x < 4$) due to preferential removal of oxygen anions. Sputtering of the sample for 15 min (not shown) resulted in line broadening which is an indication of reduction of some Ti^{+4} cations. Further sputtering (for 30 min, not shown) resulted in a further decrease in the relative intensity of Ti^{+4} with respect to Ti^{+x}. The XPS Ti(2*p*) region of the sample sputtered for 45 min is presented in Fig. 1b. The presence of Ti^{+3} and Ti^{+2} lines at 457.4 and 456.0 eV is a clear indication of the reduction of Ti^{+4} cations. Previous studies by XPS (67) and NEXAFS (72) of the relative concentrations of Ti cations as a function of Ar^+-sputtering time have indicated that a threshold is reached upon sputtering, with Ti^{+4} cations representing about 30% of the total Ti cations. Figure 2 shows the percentage Ti^{+4} of the fresh and Ar^+-bombarded TiO_2/CMSF. Ti^{+x} lines at 457.4, and 455.9 (±0.1) eV were attributed to Ti^{+3} and Ti^{+2} cations, respectively (67, 72–74). Similar results on TiO_2 (001) single crystal from reference (67) are also presented in Fig. 2. The percentage of Ti^{+4} cations at prolonged sputtering time is very similar for both materials. The discrepancy between the Ti cations distribution in TiO_2/CMSF and TiO_2 (001) single crystal at short sputtering times may be related to different experimental conditions. In both experiments the emission current (25 mA) and Ar partial pressures (5×10^{-7} Torr, differential pumping) were the same, while sample position to the analyzer and accelerating voltage were different.

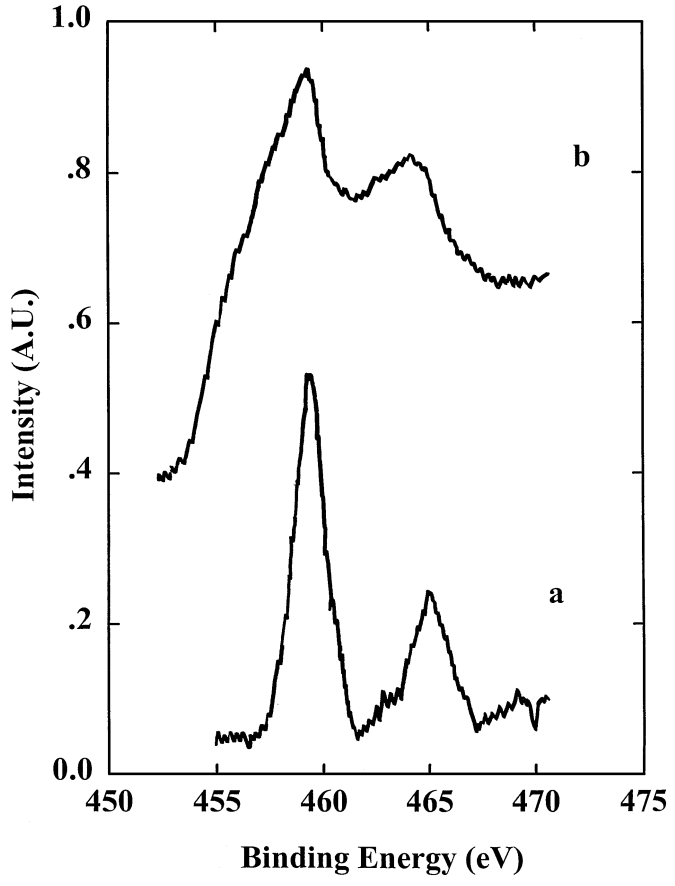

FIG. 1. XPS Ti(2*p*) of annealed TiO_2/CMSF and Ar^+-sputtering TiO_2/CMSF.

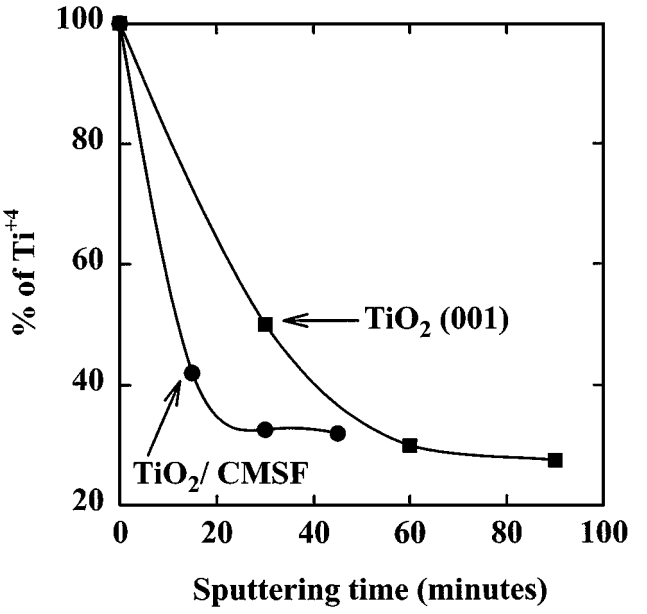

FIG. 2. Percentage of Ti^{+4} cations as a function of Ar^+-sputtering time over TiO_2/CMSF, and TiO_2 (001) single crystal (from Ref. (67)).

2. UV–Visible Diffuse Reflectance

Figure 3 presents UV–vis diffuse reflectance spectra of TiO_2 (anatase) and TiO_2/CMSF. A blue shift in the band-gap of ca. 50 nm is observed for TiO_2/CMSF when compared to TiO_2 (anatase). This value corresponds to an increase of

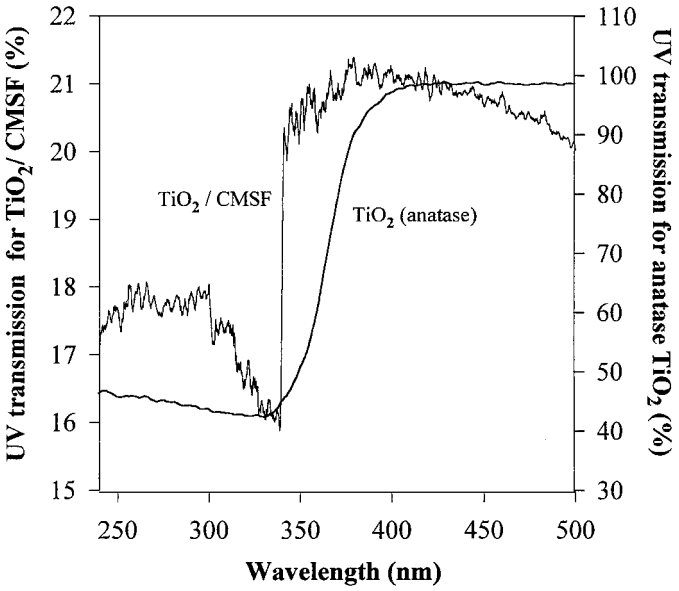

FIG. 3. UV–vis diffuse reflectance of TiO_2 (powder) and TiO_2/CMSF.

band-gap energy of 0.6 to 0.7 eV ($1\ \text{eV} = 1.23 \times 10^3/\lambda\ (\text{nm})$). This is due to a considerable decrease in the particle dimension. XRD has been conducted on this material and has shown no evidence of TiO_2 diffraction lines, confirming the considerable decrease in particle dimensions. If we assume that the absorbance energy shift is equivalent to the energy shift, ΔE, of the band-gap of TiO_2 particles one can calculate the particle radius of TiO_2 in CMSF. ΔE is a function of the three-dimensional confinement model based on the effective mass approximation (75–77),

$$\Delta E = \{\hbar^2\pi^2/2r^2\}[(1/m_e^*) - (1/m_h^*)] - 1.786e^2/\varepsilon r - 0.24E_{Ry}, \quad [1]$$

where ΔE is the change in the band-gap with particle dimension, r is the particle radius, m_e^* and m_h^* are the effective masses for the electrons and holes, ε is the dielectric constant, and E_{Ry} is the effective Ryberg energy (which is small). The first term represents the energy of localization, the second represents the Coulombic attraction, and the third represents the correlation effects. The computed value of r is equal to 15 ± 2 Å (calculations were performed with $\varepsilon = 87$, $m_e^* = 0.24\ m_e$ (m_e is the electronic rest mass) and $m_h^* = 0.45\ m_e$; E_{Ry} is neglected). Particles of radius between 50 and 70 Å were observed by TEM (×230 000). This is four to five times higher than the calculated values by UV–vis experiments. Energy dispersive analysis associated with the TEM was not available and we could not obtain good contrast with higher magnification. In the absence of further data we cannot claim for sure that these particles are those of TiO_2 clusters. Since XPS has shown the absence of any other materials then one may consider that these particles are TiO_2 clusters outside the pores.

3. Ethanol Reactions at Atmospheric Pressure on TiO_2/CMSF and TiO_2 Powder

Figure 4a presents ethanol reaction on TiO_2 (mainly anatase) powder. The fast ethanol reaction is concomitant with the formation of considerable amounts of acetaldehyde. Acetaldehyde is then further decomposed ultimately to CO_2. To obtain reliable kinetic information the amount of ethanol was kept small ($\approx 10^{-8}$ mol/ml) and thus we could not follow the CO_2 evolution because it is well below the detection limit of a TCD. However, one of the authors has previously followed the amount of CO_2 produced (16, 17, 37) on the same powder material (using an FID connected

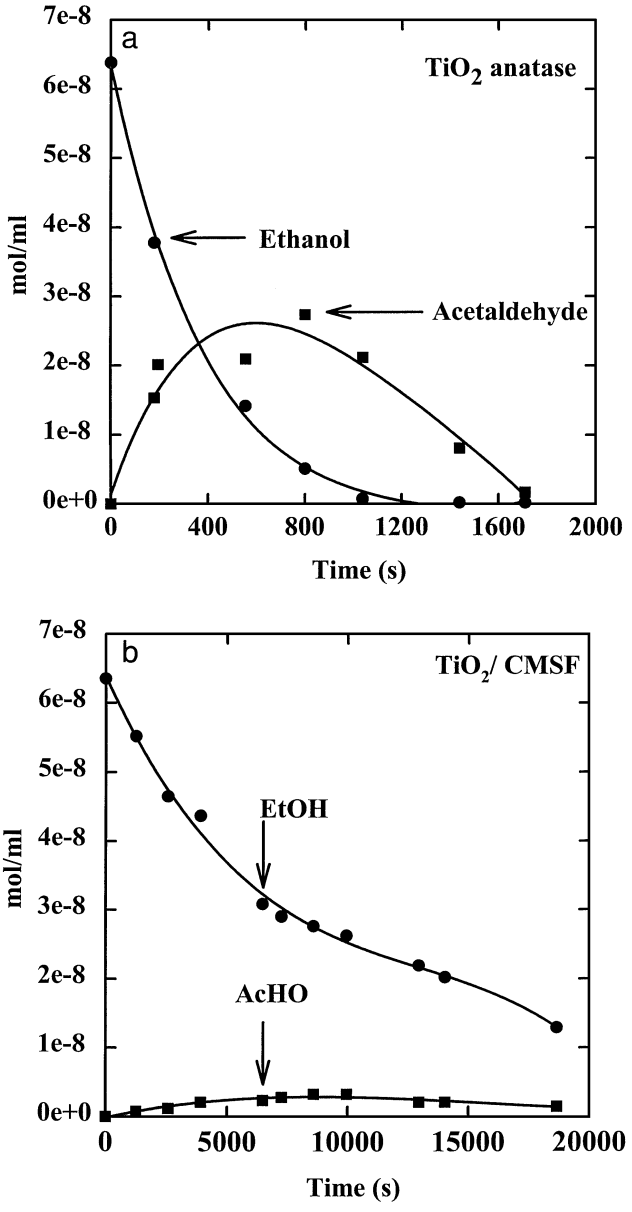

FIG. 4. Ethanol reactions, at 1 atm, over (a) TiO_2 (anatase), 25 mg, and (b) TiO_2/CMSF, 150 mg.

to a CO_2-to-methane reactor) and has shown that one can explain the reaction in a sequential way as follows:

$$CH_3CH_2OH \xrightarrow{k_1K_1} CH_3CHO \xrightarrow{k_2K_2} 2\,CO_2 \qquad [2]$$

It has also been shown (16, 17, 37) that the reaction follows Langmuir–Hinshelwood kinetics,

$$r_{\text{ethanol}} = k_1K_1\,[\text{ethanol}]/(1 + K_1\,[\text{ethanol}]), \qquad [3]$$

where r_{ethanol} is the rate of consumption of ethanol in mol/g s, k_1 is the rate constant, and K_1 is the binding constant. This is in agreement with results obtained by other workers for the photodecomposition of ethanol as well as other organic compounds (8, 10, 38). From Fig. 4a k_1K_1 is calculated equal to 24.3 ml/g s. One can calculate the rate k_2K_2 (neglecting K[ethanol] since [ethanol] $\ll 1$) as

$$r_{\text{acetaldehyde}} = k_1K_1\,[\text{ethanol}] - k_2K_2\,[\text{acetaldehyde}]. \qquad [4]$$

From Fig. 4a k_2K_2 is equal to 4.5 ml/g s. However, one can also obtain k_2K_2 from the reaction of acetaldehyde on TiO_2 in a separate run. This is presented in Fig. 5 where k_2K_2 is found equal to 1.4 ml/g s (this value is more accurate since it is computed from the slope of the curve averaging several data points).

Figure 5b presents the corresponding reaction of ethanol to acetaldehyde on TiO_2/CMSF. There are two main differences. First, the reaction rate constant is slower. This is expected since the material contains ca. 5 wt% TiO_2. Second, ethanol decomposition is associated with a noticeable small formation of acetaldehyde; in other words, the rate constant for acetaldehyde decomposition into CO_2 is far greater than that of ethanol to acetaldehyde. From Fig. 4b the rate constant k_1K_1 for ethanol decomposition to acetaldehyde is computed equal to 0.053 ml/g s. From Fig. 5, presenting the reaction of acetaldehyde on TiO_2/CMSF, k_2K_2 is equal to 0.13 ml/g s. Thus, the comparison between both rate constants (for ethanol and acetaldehyde decomposition) on both catalysts (TiO_2 and TiO_2/CMSF) clearly shows that TiO_2/CMSF is far more selective for the total decomposition of ethanol to CO_2. The ratio k_1K_1/k_2K_2 for both catalysts is presented in Table 1. A higher ratio indicates the accumulation of high concentrations of acetaldehyde and a lower ratio indicates high selectivity to total decomposition. It is worth mentioning that no evidence of deactivation of the TiO_2/CMSF was observed. The total run-time conducted on TiO_2/CMSF is about 90 h (17 experiments).

TABLE 1

Ratio of Rate Constants of the Photoreaction of Ethanol to CO_2 over TiO_2 and TiO_2/CMSF

Catalyst	$(k_1K_1)/(k_2K_2)$
TiO_2	17.4
TiO_2/CMSF	0.4

Note. k_1K_1, CH_3CH_2OH to CH_3CHO; k_2K_2, CH_3CHO to CO_2.

4. Ethanol Reactions in UHV on TiO_2/CMSF

The photoreaction of ethanol has been conducted on TiO_2/CMSF in UHV. The sample was cleaned as described in the Experimental section. The main three products observed were acetaldehyde, ethylene, and CO_2. Several runs were conducted both at room and higher temperatures. For data analysis the CO_2 chamber background has been subtracted as well as the fragments of ethanol at m/e 29 (24% of that of m/e 31) and m/e 27 (23% of that of m/e 31). Figure 6 shows the relative yield of acetaldehyde (m/e 29), ethylene (m/e 27), and CO_2 (m/e 44; the m/e 44 contribution of acetaldehyde has been subtracted) for the dark reaction at

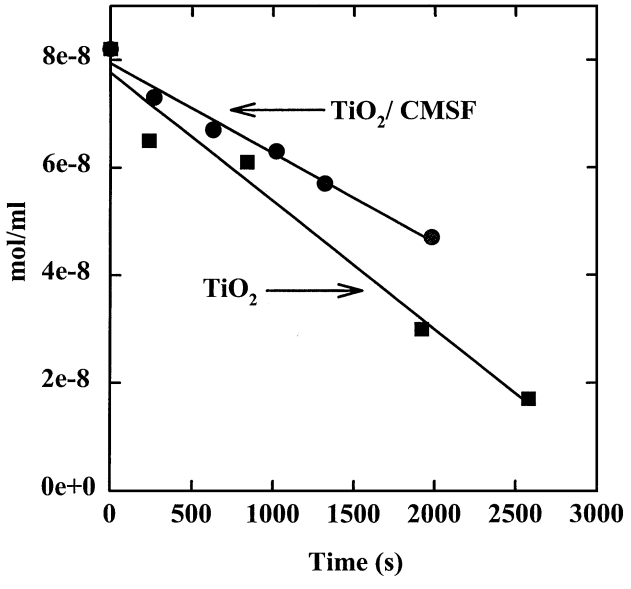

FIG. 5. Acetaldehyde reactions, at 1 atm, over TiO_2 (anatase), 25 mg, and TiO_2/CMSF, 150 mg.

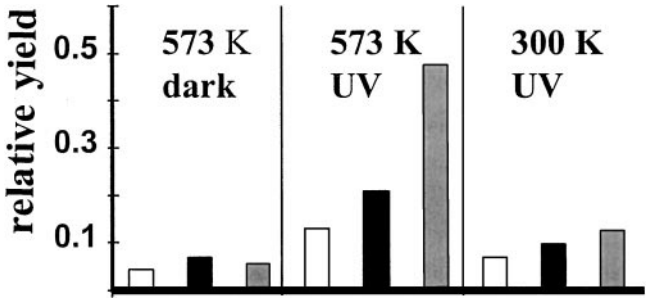

FIG. 6. Relative yield of acetaldehyde ((m/e 29)/(m/e 31); white), ethylene ((m/e 27)/(m/e 31); black), and CO_2 ((m/e 44)/(m/e 31); grey) for ethanol reactions over TiO_2/CMSF at ca. $5 \pm 1 \times 10^{-7}$ Torr.

573 K, the UV reaction at 300 K, and the UV reaction at 573 K of ethanol over TiO_2/CMSF. Ethanol pressure was kept constant for all runs, at $5 \pm 1 \times 10^{-7}$ Torr. At room temperature (not shown) no reaction of ethanol was observed in the absence of UV. CO_2 is the major reaction product with UV while acetaldehyde is the major reaction product under dark conditions. At 573 K, in the presence of UV, the formation of CO_2 increased eightfold while that of acetaldehyde increased threefold when compared to dark conditions.

5. Temperature Programmed Desorption (TPD) after Ethanol Adsorption at Room Temperature over TiO_2/CMSF

Figures 7 and 8 present ethanol-TPD of TiO_2/CMSF under dark and UV excitation, while Tables 2 and 3 show the carbon yield and selectivity of these TPDs. Ethanol (m/e 31) desorbs at 480 K followed by CO_2 (m/e 44). Acetaldehyde (m/e 29) desorbs at 535 and 565 K under dark and UV conditions, respectively. Ethylene (m/e 27) desorbs in the same temperature domain, ca. 550 K, under both conditions. Both ethylene and acetaldehyde contributed by similar amounts (see Tables 2 and 3 for C selectivities). With the exception of increasing ethanol conversion about 12%, no major differences were observed between UV and dark conditions. In both cases no carbon–carbon bond formation was observed. Figure 9 shows ethanol-TPD on TiO_2/CMSF that has been annealed in the presence of O_2, prior to ethanol adsorption at room temperature. Also shown in Table 4 are the carbon yields and selectivity of this TPD. One important point is worth mentioning; the reaction selectivity switches from equal amounts of acetaldehyde (a product of ethanol dehydrogenation) and ethylene (a product of ethanol dehydration) to a ratio of acetaldehyde to ethylene of ca. 3. In other words, annealing TiO_2/CMSF with O_2 favors the dehydrogenation reaction of ethanol. A second observation, although less dramatic, is related

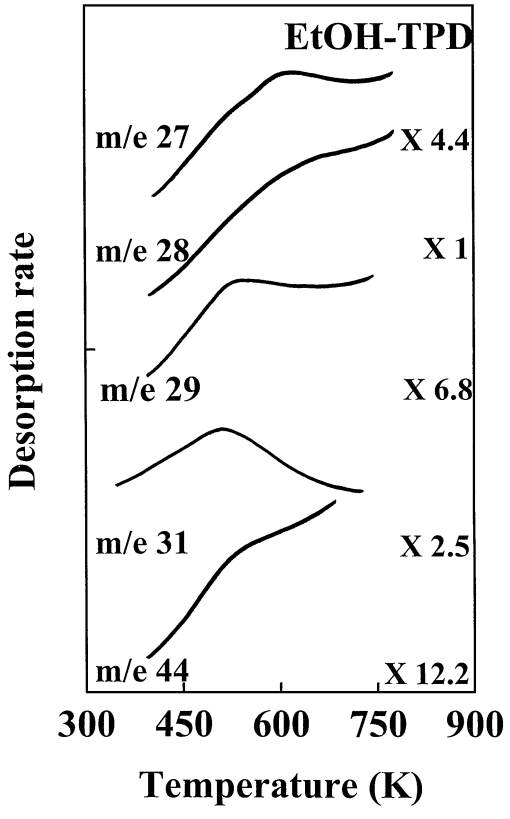

FIG. 7. Temperature programmed desorption after ethanol adsorption at 310 K over TiO_2/CMSF in absence of UV.

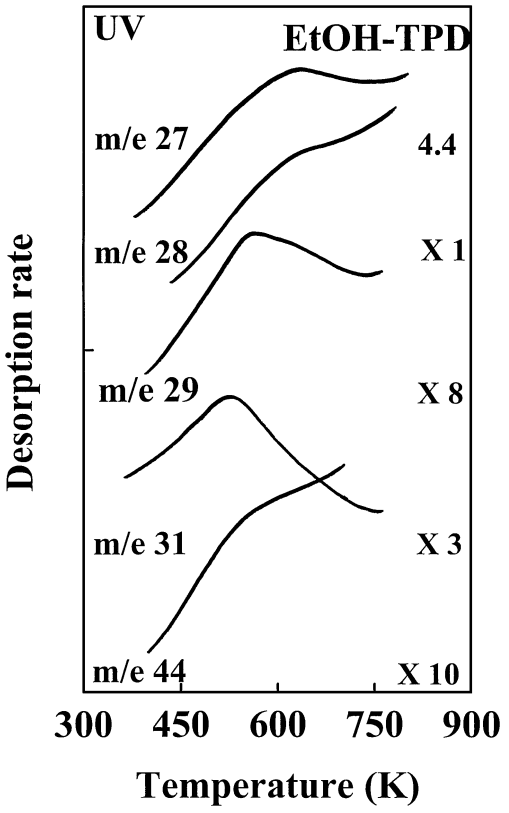

FIG. 8. Temperature programmed desorption after ethanol adsorption at 310 K over TiO_2/CMSF in presence of UV.

TABLE 2

Carbon Yield and Selectivity of Temperature Programmed Desorption after Ethanol Adsorption at 310 K over TiO_2/CMSF in Absence of UV

Product	Peak temperature (K)	Carbon yield (%)	Selectivity (%)
Acetaldehyde (m/e 29)	535	26.5	49
Ethanol (m/e 31)	485	46.2	
CO_2 (m/e 44)	525	2.2	4
Ethylene (m/e 27)	545	25.1	47

TABLE 3

Carbon Yield and Selectivity of Temperature Programmed Desorption after Ethanol Adsorption at 310 K over TiO_2/CMSF in Presence of UV

Product	Peak temperature (K)	Carbon yield (%)	Selectivity (%)
Acetaldehyde (m/e 29)	565	28.8	47.5
Ethanol (m/e 31)	480	39.3	
CO_2 (m/e 44)	550	2.1	3.5
Ethylene (m/e 27)	555	29.8	49

TABLE 4

Carbon Yield and Selectivity of Temperature Programmed Desorption after Ethanol Adsorption at 310 K over Prior-Annealed TiO_2/CMSF with O_2 (12×10^3 L), in Presence of UV

Product	Peak temperature (K)	Carbon yield (%)	Selectivity (%)
Acetaldehyde (m/e 29)	570–610	41	69
Ethanol (m/e 31)	520	40.5	
CO_2 (m/e 44)	530	5.5	9
Ethylene (m/e 27)	610	13	22

to CO_2 formation. Annealing in O_2 prior to TPD doubled CO_2 desorption. Both dark and photocatalytic reactions will require removal of either lattice O anions or adsorbed O anions to make CO_2. Thus, it is not surprising that O_2 prior treatment of the material resulted in enhancing CO_2 formation.

Since acetaldehyde is the main reaction product of Ethanol-TPD as well as a product of partial oxidation of ethanol under UV under steady state conditions it is thus worth investigating the reactions of acetaldehyde by TPD.

6. Temperature Programmed Desorption (TPD) after Acetaldehyde Adsorption at Room Temperature on TiO_2/CMSF

Figure 10 and Table 5 present the desorption products as well as carbon conversion and selectivity, respectively, of acetaldehyde–TPD on TiO_2/CMSF in the absence of UV. Unreacted acetaldehyde desorbed in two temperature domains at 430–440 and at ca. 650 K. Both desorptions contributed 46.0% of the total carbon yield.

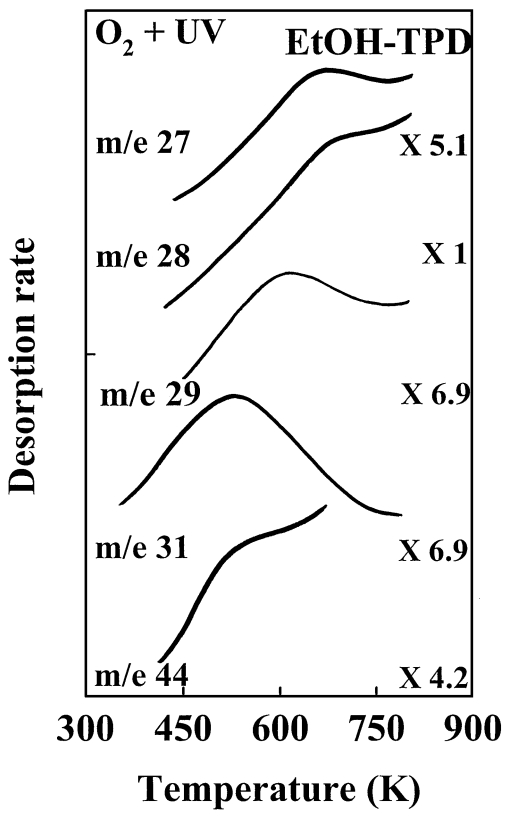

FIG. 9. Temperature programmed desorption after ethanol adsorption at 310 K over TiO_2/CMSF, that has been prior annealed with O_2 (12×10^3 L), in presence of UV.

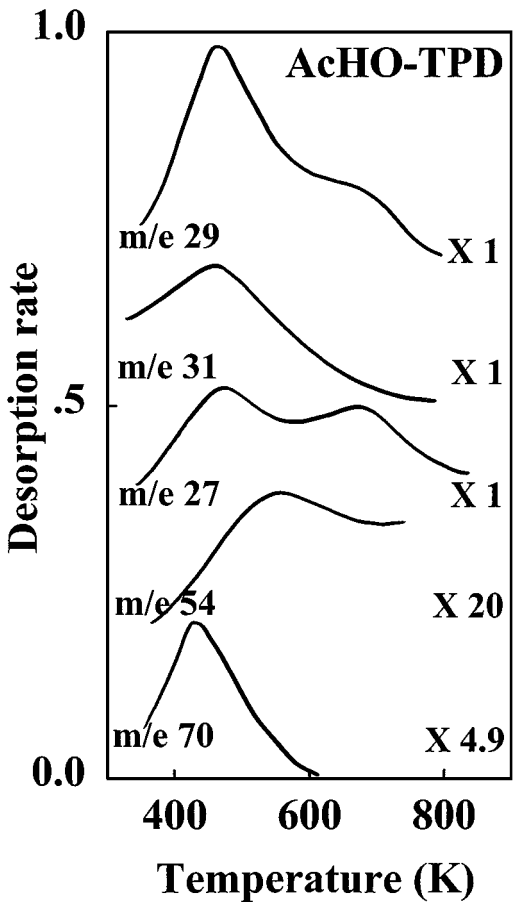

FIG. 10. Temperature programmed desorption after acetaldehyde adsorption at 310 K over TiO_2/CMSF in absence of UV.

TABLE 5

Carbon Yield and Selectivity of Temperature Programmed Desorption after Acetaldehyde Adsorption at 310 K over TiO_2/CMSF in Absence of UV

Product	Peak temperature (K)	Carbon yield (%)	Selectivity (%)
Acetaldehyde (m/e 29)	430–440	30.1	
Acetaldehyde (m/e 29)	650	15.9	
Ethanol (m/e 31)	480	24.4	45.3
Ethylene (m/e 27)	690	6.3	11.7
Butadiene	550–560	3.1	5.7
Crotonaldehyde (m/e 70)	440–450	17.9	33
Crotyl alcohol (m/e 72)	440–450	2.3	4.3

Evidence of acetaldehyde reduction was obtained from ethanol desorption at 480 K and contributed by 24.4%, carbon yield. In addition, ethylene (m/e 27) was observed at 690 K (6.3%). Ethylene desorption most likely resulted from the dehydration of small amounts of ethanol. Evidence of C–C bond formation was also observed. Crotonaldehyde (m/e 70, 55, and 39) and crotyl alcohol (m/e 72, 71, and 57) desorbed at 440–450 K and both contributing by 20.2% carbon yield. Crotonaldehyde is formed by β-aldolization of two molecules of acetaldehyde followed by dehydration (no evidence of the aldol product was observed, absence of m/e 88). Crotyl alcohol is formed by reduction of adsorbed crotonaldehyde species. Both crotonaldehyde and crotyl alcohols were observed previously on TiO_2 (001) single crystal and TiO_2 powder (65) during acetaldehyde-TPD and on TiO_2 powder during steady state reactions (36). Small amounts of butadiene were also observed (C selectivity 5.7%). Butadiene desorption was detected during ethanol-TPD on TiO_2 (anatase) (40) and during acetaldehyde-TPD on TiO_2 (001) single crystal and TiO_2 powder (65).

Figure 11 and Table 6 show the desorption products as well as carbon conversion and selectivity, respectively, of

TABLE 6

Carbon Yield and Selectivity of Temperature Programmed Desorption after Acetaldehyde Adsorption at 310 K over TiO_2/CMSF in Presence of UV

Product	Peak temperature (K)	Carbon yield (%)	Selectivity (%)
Acetaldehyde (m/e 29)	430	38.4	
Acetaldehyde (m/e 29)	650	10.4	
Ethanol (m/e 31)	430	9	17.5
Ethanol (m/e 31)	540	11	21.4
Crotonaldehyde (m/e 70)	460	20.3	39.4
Butadiene (m/e 54)	560	5.9	11.4
Formaldehyde (m/e 30)	450	5.3	10.3

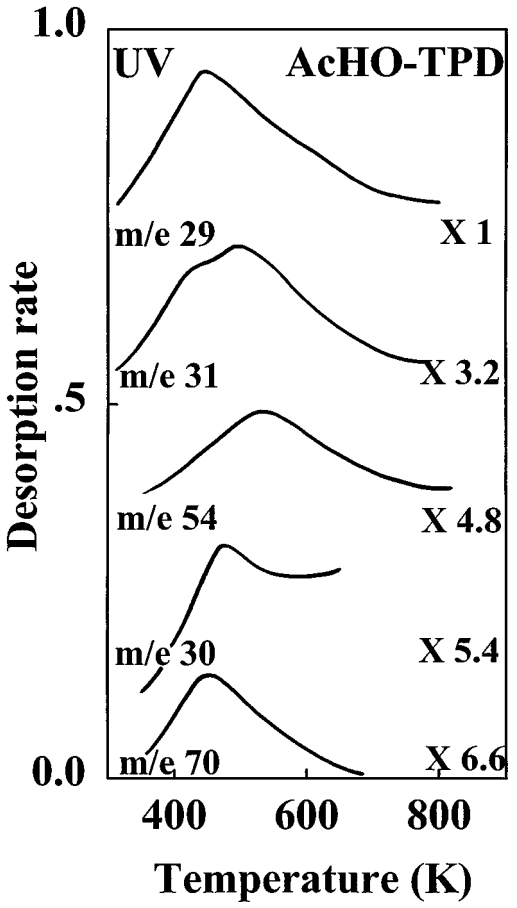

FIG. 11. Temperature programmed desorption after acetaldehyde adsorption at 310 K over TiO_2/CMSF in presence of UV.

acetaldehyde-TPD on TiO_2/CMSF in the presence of UV illumination. Acetaldehyde desorbed in two temperature domains (similar to dark-TPD) at 430 and 650 K. The second desorption is, however, considerably small. Unlike dark-TPD ethanol desorbed in two temperature domains at 430 and 540 K. The overall carbon yield of ethanol is, however, comparable to that of dark-TPD (20.0%). Similar to dark-TPD, crotonaldehyde desorbed at 460 K, with a carbon yield of 20.3%. One major difference between dark- and UV-TPD is, however, noted: formaldehyde (m/e 30) desorbed at 450 K with a C selectivity of 10.3%. Butadiene (m/e 54) desorbed at 560 K with a C selectivity of 11.4% (more than twice in the absence of UV). Ethylene desorption in the presence of UV was not observed. Butene and butadiene formation from acetaldehyde has been previously studied in detail on TiO_2 surfaces and is due to reductive coupling of two adsorbed acetaldehyde molecules on reduced Ti cation centers (i.e., Ti^{+x} with $x < 4$) (59, 60). This is, in fact, an important observation since it indicates that during UV excitation, where Ti^{+3} cations and holes are formed, the reductive coupling of acetaldehyde is enhanced (twofold) due to the increase of these Ti^{+3} centers.

DISCUSSION

The following results were obtained from this study.

1. XPS Ti(2*p*) lines of TiO_2/CMSF as well as Ar^+-sputtered TiO_2/CMSF indicate similar behavior to that of TiO_2 single crystals.

2. UV-vis diffuse reflectance indicates a blue shift of the absorbance of TiO_2/CMSF when compared to TiO_2 powder. This blue shift of 0.6–0.7 eV corresponds to an average decrease of particle radius to ca. 15 ± 2 Å.

3. Kinetics at atmospheric pressure shows that k_2K_2/k_1K_1 of TiO_2/CMSF is about 40 times higher than that of TiO_2 powder. This indicates the high selectivity of TiO_2/CMSF when compared to TiO_2 powder for the decomposition of acetaldehyde.

4. Steady state kinetics in UHV shows eightfold increase of CO_2 with UV, at 573 K, when compared to dark reaction at the same temperature.

5. Ethanol-TPD indicates that prior annealing of TiO_2/CMSF with O_2 resulted in switching the reaction selectivity from equal amounts of acetaldehyde and ethylene to a 3 to 1 ratio of acetaldehyde to ethylene.

6. Acetaldehyde-TPD shows formaldehyde desorption in presence of UV. Moreover, the reductive coupling of two molecules of acetaldehyde followed by dehydrogenation to butadiene is enhanced (twofold) by UV excitation.

The dark reaction of ethanol on TiO_2 has been studied by several workers. On TiO_2 anatase Kim *et al.* (14) observed several desorption products: acetaldehyde (dehydrogenation), diethylether (dehydration), ethylene (dehydration), and butene (coupling). The authors explained ether formation due to a bimolecular interaction between adsorbed alkoxides, while that of ethylene by cleavage of the β C–H and C–O bonds. The formation of surface oxygen vacancies (due to removal of water at 390 K) drives the C–O bond dissociation. On TiO_2 (001) single crystal, unlike powder work (14), the main reaction of ethanol was dehydration to ethylene; the ratio ethylene (dehydration) to acetaldehyde (dehydrogenation) = 4.75 (13). No considerable differences in ethanol reactivity are observed (40) on anatase and rutile TiO_2. However, the initial coverage of the surface and the amount of surface hydroxyls have dramatic effects on the reaction selectivity (78). The selectivity to ethylene increases with decreasing ethanol coverage in detriment to that of C_4H_6 and C_4H_8. Hydroxylation (either post or prior to ethanol adsorption) of the surface resulted in decreasing adsorbed ethanol populations. Gamble *et al.* (79) investigated the decomposition pathways of ethanol on TiO_2 (110) single crystal. Unlike TiO_2 powder and TiO_2 (001) single crystal works (13, 14, 40, 78) they do not observe evidence of acetaldehyde formation; ethylene is the only observed reaction product on both stoichiometric and Ar^+-sputtered surfaces (79). The adsorption and dissociation of ROH molecules on the surface of TiO_2 (110) have been studied by density-functional theory and the pseudopotential method (80). For the most favorable molecular mode of adsorption the adsorption energy is very close to that for dissociative adsorption.

The photoreaction of ethanol on the surfaces of TiO_2 powder was also studied by several workers. Ethanol is photo-decomposed to CO_2 through several reaction intermediates such as acetaldehyde (37), formaldehyde (38), formic acid (18), and acetic acid (18). In all studies considerable concentration of aldehydes is observed. Sauer and Ollis (38) also conducted a detailed kinetic study for ethanol and acetaldehyde photo-oxidation on TiO_2 coated on a nonporous quartz plate and on a porous ceramic honeycomb monolith in humidified air. They found that the type of support is critical: the former contained only illuminated (active) surfaces, while the latter consisted of substantial dark surfaces coated with a thin layer of illuminated catalyst. Idriss *et al.* studied the effect of humidity on the photo-oxidation of ethanol (17) and acetaldehyde (37) on TiO_2. The rate of reaction of ethanol decomposition as a function of percent humidity shows a bimolecular surface reaction with rate enhancement of ca. 50% at low percent humidity—similar behavior has also been observed by Peral and Ollis (81). The effect of humidity was more dramatic for acetaldehyde decomposition with a fivefold and threefold increase on TiO_2 (anatase/rutile) and TiO_2 (anatase), respectively at low percent humidity (37). Muggli *et al.* (18) conducted a detailed mechanistic study of the photocatalytic oxidation of ethanol on TiO_2. They proposed two parallel reaction pathways for acetaldehyde (from ethanol). The first consists of acetaldehyde $\rightarrow$ acetic acid $\rightarrow$ CO_2 while the second follows formaldehyde (from acetaldehyde) $\rightarrow$ formic acid $\rightarrow$ CO_2. The authors (18) claim the detection of acetic acid during ethanol-TPD of TiO_2 which has been subject to photocatalytic decomposition for prolonged time. Acetic acid desorption in their experiment was presented by a rising desorption signal up to 723 K, with no evidence of a desorption peak. Under these conditions it is unclear whether the signal attributed to acetic acid is in fact due to a desorption product. In all cases the desorption of acetic acid during their TPD is very small. Kennedy and Datye (82) investigated the reaction of ethanol over Pt/TiO_2; although they did include in their reaction mechanism acetic acid, the authors did not follow acetic acid formation. The presence of acetic acid has been reported from the photocatalytic reaction of acetaldehyde on TiO_2 thin film under UV illumination (83). The authors followed CO_2 and acetaldehyde by GC-FID and the products remaining (presumably adsorbed carboxylic acid or carboxylate species) on the surface extracted by 0.01 NaOH solution and measured using a liquid chromatograph with a UV-8010 optical detector (83). We do not observe (in this work) evidence of acetic acid desorption during UV-TPD

and we have not extracted the reaction products remaining on the surface after steady state condition or after batch reactions.

From the above observations and the present work one can present the reaction mechanism of ethanol and acetaldehyde over TiO_2/CMSF as follows.

A. Dark Reactions of Ethanol

Adsorbed ethanol molecules at room temperature undergo O–H bond dissociation on Ti–O centers to yield ethoxy species

$$CH_3CH_2OH\ (g) \rightarrow CH_3CH_2OH\ (a)\ \text{at ca. 300 K (adsorption)} \quad [5]$$

$$CH_3CH_2OH\ (a) + O\ (l) \rightarrow CH_3CH_2O\ (a) + OH\ (a)\ \text{at 300 K (dissociation)} \quad [6]$$

(g), gas; (a), adsorbed; (l), lattice.

Part of ethoxy species recombine with protons, from OH (a) and give back ethanol during TPD.

$$CH_3CH_2O\ (a) + OH\ (a) \rightarrow CH_3CH_2OH\ (g)\ \text{at 450–500 K} \quad [7]$$

Another fraction of ethoxy species undergo H elimination and yield acetaldehyde.

$$CH_3CH_2O\ (a) \rightarrow CH_3CHO\ (a) + H(a) \quad [8]$$

$$CH_3CHO\ (a) \rightarrow CH_3CHO\ (g)\ \text{at 530–560 K} \quad [9]$$

The remaining ethoxy species undergo dehydration to yield ethylene.

$$CH_3CH_2O\ (a) \rightarrow CH_2{=}CH_2\ (g) + OH\ (a)\ \text{at 550–610 K} \quad [10]$$

TPD data shows that the ratio ethylene to acetaldehyde is 0.96. This indicates that the "stoichiometric TiO_2"/CMSF may contain equal amounts of sites responsible for dehydrogenation as well as dehydration reactions, far higher than TiO_2 (001) single crystal (13), and TiO_2 (anatase) (14); TiO_2 (110) does not yield any acetaldehyde (79). In the presence of excess O (prior annealing and cooling—10^{-5} Torr/20 min—in presence of O_2) a shift of ethylene to acetaldehyde ratio from 0.96 to 0.32 is observed. Clearly excess oxygen has switched Eq. [10] to the left, most likely by restoring surface point defects–oxygen anions vacancies.

B. Ethanol Reactions under UV Illumination

When TiO_2 is excited with UV photons having energy equal to (or higher than) its band-gap, electron transfer form the valence band to the conduction will occur.

$$TiO_2 + UV \rightarrow e^- + h^+ + TiO_2 \quad [11]$$

Upon ethanol adsorption, steps [5] and [6], hydroxyls and ethoxy species are formed. OH (a) reacting with h^+ will result in the formation of OH radicals.

$$h^+ + OH\ (a) \rightarrow {}^{\bullet}OH \quad [12]$$

OH radicals may react with adsorbed ethoxy species to yield adsorbed acetaldehyde radicals which may lose an electron and desorb.

$${}^{\bullet}OH + CH_3CH_2O\ (a) \rightarrow CH_3C^{\bullet}HO\ (a) + H_2O \quad [13]$$

$$CH_3C^{\bullet}HO\ (a) \rightarrow CH_3CHO\ (a) + e^- \quad [14]$$

Acetaldehyde may also be oxidized to acetic acid which in turn is decomposed to CO_2 (18, 18a).

$$CH_3CHO + {}^{\bullet}OH \rightarrow CH_3CO^{\bullet} + H_2O \quad [15a]$$

$$CH_3CO^{\bullet} + {}^{\bullet}OH \rightarrow CH_3COOH \quad [15b]$$

$$2\,CH_3COOH + O_2 \rightarrow CO_2 + 4\,H_2O \quad [15c]$$

We have looked for acetic acid by TPD (this work); no evidence of its formation has been observed. Under steady state conditions step [14] is minor on TiO_2/CMSF but important on TiO_2 powder. In TPD experiments, with the exception of ethylene and CO_2 we do not observe any other desorption (among the investigated products that were not detected are formic acid, acetic acid, methanol, and formaldehyde). The fact that acetaldehyde formation (under batch conditions, 1 atm) on TiO_2/CMSF is far smaller than that of TiO_2 (see Fig. 4) indicates that steps [15a]–[15c] (or similar steps) are major reaction pathways. Several reasons might be behind this. First, small particle size may have a stronger binding energy than larger particles and that may play a role in stabilizing acetaldehyde enough for further decomposition. Evidence of stronger binding energy of adsorbates on small particles when compared to larger ones has been reported on metals; for example, the strength of adsorption of H, OH, and CO increased with decreasing particle size of Pt (84). Second, step [14] will be favored on nondiffusion limited desorption such as on TiO_2 powder where micropores are on the order of 400 Å, while on CMSF, with micropores on the order of 5 Å, diffusion limited desorption will occur enhancing further reactions and thus decomposition. A similar effect was previously shown by Landau *et al.* (85): Pt catalysts on this same material (CMSF) demonstrated shape-selective reaction where competitive hydrogenation of 1-hexene and cyclohexene resulted in significantly higher rates of hydrogenation of the former rather than the latter. Both factors, stronger binding energy and slow diffusion, will favor further oxidation steps.

C. Dark Acetaldehyde Reactions over TiO_2/CMSF

Of adsorbed acetaldehyde molecules, 46% desorb unreacted. The remaining molecules give ethanol (24.4%, at 480 K), crotonaldehyde (17.9%, at 450 K), crotyl alcohol (2.3%, at 450 K), and ethylene (6.5%, at 690 K). Crotonaldehyde is formed via aldolization of two molecules of acetaldehyde. TiO_2 powder is an active catalyst for aldolization reactions (36, 65, 86) and both C4 products were previously observed on TiO_2 powder and single crystal works (65, 36). In that respect TiO_2/CMSF is similar to TiO_2 powder. The TPD selectivity is, however, dramatically different. Powder and single crystal TiO_2 show 80% + conversion to C4 containing molecules (36, 65, 86), while the present study shows only ca. 20%. Pore dimensions are the most likely explanation. The bulky precursor to crotonaldehyde (adsorbed aldol molecule) as well as adsorbed crotonaldehyde may not desorb or may undergo further aldolization reactions, due to very slow diffusion. Since TEM has shown evidence of some particles outside the pores, it is reasonable to assume that β-aldolization occurs over these particles rather than over small TiO_2 particles inside the pores. [The reaction mechanism for β-aldolization reactions over TiO_2 has been presented and discussed previously (65, 36).] Ethanol formation results from the reaction of adsorbed acetaldehyde with hydrogen atoms; the latter are provided, among others, by the aldolization steps (which starts by abstraction of a hydrogen atom, in the alpha position of the carbonyl group, by lattice oxygen anions). Ethylene is most likely formed from traces of ethanol after acetaldehyde reduction.

D. Acetaldehyde Reactions in Presence of UV

The most important observations are related to the enhancement of butadiene desorption and the formation of formaldehyde under UV on nonreduced TiO_2/CMSF. As shown in step [11] upon excitation with UV, electron transfer from O(2*p*) to Ti(3*d*) levels occurs. This results in partial reduction of Ti^{+4} cations.

$$e^- + Ti^{+4} \rightarrow Ti^{+3} \qquad [16]$$

The presence of Ti^{+3} cations under UV photons has been reported by several researchers (78–80). Ti^{+4} cations are also reduced to Ti^{+3} and other Ti cations in the suboxide form by Ar^+-sputtering (this work, 67–74). The presence of Ti suboxides is responsible for the reductive coupling of carbonyls to symmetric olefins (87, 88). The formation of butadiene is due to traces of Ti^{+3} cations present on the surface. The increase of butadiene yield during TPD under UV is evidence of the increase in these Ti^{+3} cations (step [16]). In light of that, the proposed reaction pathway is given:

$$4\,Ti^{+3} + 2\,CH_3CHO \rightarrow CH_3CH{=}CHCH_3 + 4\,Ti^{+4} + 2\,O^{2-} \qquad [17]$$

$$CH_3CH{=}CHCH_3 \rightarrow CH_2{=}CHCH{=}CH_2 + 2\,H\ (a) \qquad [18]$$

The presence of formaldehyde desorption is evidence of C–C bond dissociation and is consistent with other findings showing formaldehyde to formic acid to CO_2 reaction pathway. We have not detected formic acid by TPD (although it is important to mention that both formic acid and ethyl alcohol have molecular weight of 46, both give m/e 46, 45, and 29, and thus small amounts of formic acid cannot be ruled out).

In summary, this work presents the reactions of ethanol and acetaldehyde over TiO_2/CMSF. The formation of quantum-sized TiO_2 particles is evidenced by a considerable blue shift of the band gap ($\Delta E = 0.6$–0.7 eV). The comparison between the reactivity of ethanol over this material with that over TiO_2 powder indicated the high selectivity of the former toward total decomposition of ethanol to CO_2, with minor amounts of acetaldehyde. Acetaldehyde-TPD of TiO_2/CMSF, under UV irradiation, showed the formation of formaldehyde. Moreover, a twofold increase of butene (the reductive coupling product), during UV irradiated TPD of acetaldehyde, over TiO_2/CMSF is due to increasing numbers of Ti^{+x} cations ($x < 4$).

REFERENCES

1. Al-Ekabi, H., and Serpone, N., *J. Phys. Chem.* **92**, 5726 (1988).
2. Kutsuna, S., Ebihara, Y., Nakamura, K., and Ibusuki, T., *Atm. Envi.* **27A**, 599 (1993).
3. Nosaka, Y., Sasaka, H., Norimatsu, K., and Miyama, H., *Chem. Phys. Lett.* **105**, 456 (1984).
4. Augugliaro, V., Palmisano, L., Scheavello, M., and Scalfani, A., *Appl. Catal.* **69**, 323 (1991).
5. Lu, G., Linsebigler, A., and Yates, J. T., Jr., *J. Phys. Chem.* **99**, 7626 (1995).
6. Naskar, S., Arumugom, S., and Chanda, M., *J. Photochem. Photobiol. A: Chem.* **113**, 257 (1998).
7. Anpo, M., Yamshita, H., Ichihachi, Y., and Ehara, S., *J. Electroanal. Chem.* **396**, 21 (1995).
8. Ollis, D. F., Hsiao, C.-Y., Budiman, L., and Lee, C.-L., *J. Catal.* **88**, 89 (1984).
9. Legrini, O., Oliveros, E., and Braum, A. M., *Chem. Rev.* **93**, 671 (1993).
10. Mathews, R. W., *Solar Energy.* **38**, 405 (1987).
11. Tompsett, G. A., Bowmaker, G. A., Cooney, R. P., Rodgers, K. A., and Seakins, J. M., *J. Raman Spectroscopy.* **26**, 57 (1995).
12. Kim, K. S., and Barteau, M. A., *Surf. Sci.* **223**, 13 (1989).
13. Kim, K. S., and Barteau, M. A., *J. Mol. Catal.* **63**, 103 (1990).
14. Kim, K. S., Barteau, M. A., and Farneth, W. E., *Langmuir* **4**, 533 (1988).
15. Idriss, H., and Seebauer, E. G., submitted for publication, 1999.
16. Idriss, H., and Seebauer, E. G., *J. Vac. Sci. Technol. A* **14**, 1627 (1996).
17. Idriss, H., Miller, A., and Seebauer, E. G., *Catal. Today* **33**, 215 (1997).
18. Muggli, D. S., Mccue, J. T., and Falconer, J. L., *J. Catal.* **173**, 470 (1998).

18a. Sopyan, I., Mitsuru, W., Murasawa, S., Hashimoto, K., and Fujishima, A., *J. Photochem. Photobio. A: Chem.* **98**, 79 (1996).
19. Knozinger, H., *Z. Phys. Chem., Neue Folge.* **69**, 108 (1970).
20. Rasko, J., and Solymosi, F., *J. Phys. Chem.* **98**, 7147 (1994).
21. Zhang, W. M., Desikan, A., and Oyama, S. T., *J. Phys. Chem.* **99**, 14468 (1995).
22. Alyea, E. C., Lakshmi, L. J., and Ju, Z., *Langmuir* **13**, 5621 (1997).
23. Ichikawa, M., *Bull. Chem. Soc. Jpn.* **51**, 2273 (1978).
24. Tsuji, H., Yagi, F., Hattori, H., and Kita, H., *J. Catal.* **148**, 759 (1994).
25. Rajesh, H., and Ozkan, U. S., *Ind. Eng. Chem. Res.* **32**, 1622 (1993).
26. Foster, J. J., and Masel, R. I., *Ind. Eng. Chem. Res.* **25**, 2556 (1986).
27. Noller, H., Lercher, J. A., and Vinek, H., *Mater. Chem. Phys.* **18**, 577 (1988).
28. Youssef, A. M., Khalil, L. B., and Girgis, B. S., *Appl. Catal. A* **81**, 1 (1992).
29. *Design News*, June 22, 1998.
30. Bamwenda, G. R., Tsubota, S., Nakamura, T., and Haruta, M., *J. Photochem. Photobiol. A: Chem.* **89**, 177 (1995).
31. Cuberio, M. L., and Fierro, J. L., *J. Catal.* **179**, 150 (1998).
32. Nicoll, F. H., *J. Opt. Soc. Am.* **38**, 817 (1948).
33. Anpo, M., and Kubokawa, Y., *J. Phys. Chem.* **88**, 5556 (1984).
34. Idriss, H., and Barteau, M. A., *J. Phys. Chem.* **96**, 3382 (1992).
35. Vohs, J. M., and Barteau, M. A., *Surf. Sci.* **221**, 590 (1989).
36. Rekoske, J. E., and Barteau, M. A., submitted for publication, 1998.
37. Idriss, H., and Seebauer, E. G., *Langmuir* **14**, 6146 (1998).
38. Ohon, T., Nakabeya, K., and Matsumura, M., *J. Catal.* **176**, 76 (1998).
39. Sauer, M. L., and Ollis, D. F., *J. Catal.* **158**, 570 (1996).
40. Lusvardi, V. S., Barteau, M. A., and Farneth, W. E., *J. Catal.* **153**, 41 (1995).
41. Linsbigler, A. L., Lu, G., and Yates, J. T., Jr., *Chem. Rev.* **95**, 735 (1995).
42. Rusu, C. N., and Yates, J. T., Jr., *Langmuir* **13**, 4311 (1997).
43. Kamat, P. V., *Chem. Rev.* **93**, 267 (1993).
44. Brus, L., *Appl. Phys. A* **53**, 465 (1991).
45. Weller, H., *Angew. Chem.* **32**, 41 (1993).
46. Grätzel, M., *Nature* **349**, 740 (1991).
47. Hoffmann, M. R., Martin, S. T., Choi, W., and Bahnemann, D. W., *Chem. Rev.* **95**, 69 (1995).
48. Marcus, R. A., and Sutin, N., *Biochim. Biophys. Acta* **811**, 265 (1985).
49. Marcus, R. A., *J. Phys. Chem.* **94**, 1050 (1990).
50. Lewis, N. S., *Annu. Rev. Phys.* **42**, 543 (1991).
51. Colombo, D. P., and Bowman, R. M., *J. Phys. Chem.* **99**, 11752 (1995).
52. Herron, N., Wang, Y., Eddy, M. M., Stucky, G. D., Cox, D. E., Moller, K., and Bein, T., *J. Am. Chem. Soc.* **111**, 530 (1989).
53. Wang, Y., and Herron, N., *Chem. Phy. Lett.* **200**, 71 (1992).
54. Wang, Y., Harmer, N., and Herron, N., *Isr. J. Chem.* **33**, 31 (1993).
55. Moriguchi, I., Maeda, H., Teraoka, Y., and Kagawa, S., *Chem. Mater.* **9**, 1050 (1997).
56. Koresh, J. E., Kim, T. H., and Koros, W. J., *J. Chem. Soc. Faraday Trans. 1* **85**, 1537 (1989).
57. Koresh, J. E., Kim, T. H., Walker, D. R. B., and Koros, W. J., *J. Chem. Soc. Faraday Trans. 1* **85**, 1545 (1989).
58. Koresh, J. E., Kim, T. H., Walker, D. R. B., and Koros, W. J., *J. Chem. Soc. Faraday Trans. 1* **85**, 1557 (1989).
59. Koresh, J. E., Kim, T. H., Walker, D. R. B., and Koros, W. J., *J. Chem. Soc. Faraday Trans. 1* **85**, 4311 (1989).
60. Koresh, J. E., *J. Chem. Soc. Farday Trans.* **89**, 2058 (1993).
61. Koresh, J. E., and Soffer, A., *J. Chem. Soc. Faraday Trans.* **76**, 2457 (1980).
62. Koresh, J. E., and Soffer, A., *J. Chem. Soc. Faraday Trans.* **76**, 2472 (1980).
63. Koresh, J. E., and Soffer, A., *J. Chem. Soc. Faraday Trans.* **76**, 2507 (1980).
64. Kogan, S., Landau, M. V., Herskowitz, M., and Koresh, M., *in* "Heterogeneous Catalysis and Fine Chemicals III" (Guisant *et al.*, Eds.), Elsevier, Amsterdam, 1993.
65. Idriss, H., Kim, K. S., and Barteau, M. A., *J. Catal.* **139**, 119 (1993).
66. Ko, E. I., Benziger, J. B., and Madix, M. A., *J. Catal.* **62**, 264 (1980).
67. Idriss, H., and Barteau, M. A., *Catal. Lett.* **26**, 123 (1994).
68. Idriss, H., Kim, K. S., and Barteau, M. A., *Surf. Sci.* **262**, 113 (1992).
69. Hoflund, G. B., Lin, H. L., Grogan, A. L., Asbury, D. A., Yoneyama, H., Ikeda, O., and Tamura, H., *Langmuir* **4**, 246 (1988).
70. Göpel, W., Rocker, G., and Feierabend, R., *Phys. Rev. B.* **28**, 3247 (1983).
71. Bardi, U., Tamura, K., Owari, M., and Nihei, Y., *Appl. Surf. Sci.* **32**, 352 (1988).
72. Lusvardi, V. S., Barteau, M. A., Chen, J. G., Eng, J., Fruhberger, B., and Teplyakov, A., *Surf. Sci.* **397**, 237 (1998).
73. Göpel, W., Anderson, J. A., Frankel, D., Jaehing, M., Philips, K., Schäfer, J. A., and Rocker, G., *Surf. Sci.* **139**, 333 (1984).
74. Lausmaa, J., Kasemo, B., and Matson, H., *Appl. Surf. Sci.* **44**, 133 (1990).
75. Kayanuma, Y., *Phys. Rev. B* **38**, 9797 (1988).
76. Wang, Y., Suna, A., Mahler, W., and Kasowski, R., *J. Chem. Phys.* **87**, 7315 (1987).
77. Linsebigler, A. L., Lu, G., and Yates, J. T., Jr., *Chem. Rev.* **95**, 735 (1995).
78. Lusvardi, V. S., Barteau, M. A., Dollinger, W. R., and Farneth, W. E., *J. Phys. Chem.* **100**, 1183 (1996).
79. Gambel, L., Jung, L. S., and Campbell, C. T., *Surf. Sci.* **348**, 1 (1996).
80. Bates, S. P., Kresse, G., and Gillan, M. J., *Surf. Sci.* **409**, 336 (1998).
81. Peral, J., and Ollis, D. F., *J. Catal.* **136**, 554 (1992).
82. Kennedy, J. C., III, and Datye, A. K., *J. Catal.* **179**, 375 (1998).
83. Ohko, Y., Tryk, D. A., Hashimoto, K., and Fujishima, A., *J. Phys. Chem. B* **102**, 2699 (1998).
84. Mukerjee, S., and Mcbreen, J., *J. Electroanal. Chem.* **448**, 163 (1998).
85. Landau, M. V., Kogan, S. B., Tavor, D., Herskowitz, M., and Koresh, J. E., *Catal. Today* **36**, 497 (1997).
86. Morris, D. L., US Patent: 3,948,991, Eastman Kodak Company, 1982.
87. Idriss, H., Pierce, K. G., and Barteau, M. A., *J. Am. Chem. Soc.* **116**, 3063 (1994).
88. McMurry, J. E., *Chem. Rev.* **89**, 1513 (1989). [see references therein]